Applied Numerical Modeling in Geomechanics – 2020 – Billaux, Hazzard, Nelson & Schöpfer (eds.) Paper: 17-06

Accounting for long term effects for the structural design of deep tunnels in claystones

V. Ribeiro, J.F. Bruchon & S. Burlon
Terrasol, Setec, Paris, France

1 INTRODUCTION

This paper includes the comparison of two approaches to simulate the mechanical behavior of claystones subjected to time effects for the structural design of deep tunnels that could be found for example in the Meuse/Haute-Marne Underground Research Laboratory (MHM URL) or in the Mont Terri rock laboratory. Indeed, claystones are usually sensible to time effects, which leads to consider possible significant additional structural forces for the structural design of the tunnels both in terms of normal forces and bending moments. The scatter of the structural forces may be very significantly affected by these long term effects. Besides, this structural design issue is quite important in terms of costs since it has directly an impact on the design of concrete structures in terms of thickness, class of concrete and steel ratio. In this paper, two constitutive laws are compared: the first one is based on the classical Norton law, the second one is based on an innovative approach considering a strength mobilization parameter. These two constitutive laws are calibrated and compared with experimental data from the MHM URL. Then, the comparison is extended to the structural forces into the tunnels in order to assess the scatter of these structural forces due to long term effects.

2 ACCOUNTING FOR LONG TERM EFFECTS

Long term effects in claystones, especially creep effects can be described by various approaches. In this paper, only the constitutive laws based on an implicit integration are considered using a visco-plastic potential. In this framework, based on Perzyna's theory, the very well-known Norton law is used (Boidy 2002, Souley et al. 2011, Saitta et al. 2016).

Perzyna's theory is based on the use of a visco-plastic potential with the following general equations, where $< \cdot >$ is the McCauley's brackets:

$$\dot{\epsilon}_{ij} = \dot{\epsilon}^{e}_{ij} + \dot{\epsilon}^{vp}_{ij},\ \dot{\epsilon}^{vp}_{ij} = \gamma < \Phi(F) > \frac{\partial \mathrm{f}(\sigma_{ij})}{\partial \sigma_{ij}}, where \begin{cases} < \Phi(F) > = \Phi(F), & if\ \Phi(F) > 0 \\ < \Phi(F) > = 0, & if\ \Phi(F) < 0 \end{cases} \quad (1)$$

The strain rate is divided into an elastic and a visco-plastic strain rate. The McCauley's notation indicates that Perzyna's theory supposes a purely visco-plastic material, which means that visco-plastic strains are neglected in the elastic domain. In comparison to the plasticity theory where the state of stress is unable to outstrip the yield surface, in the visco-plastic theory, the state of stress is capable to suddenly exceed the yield surface in a short-term behavior, then generates long-term strains that carry the state of stress back to yield surface (Fig. 1). Accordingly, visco-plastic strain rate depends on an overstress function Φ, a rate-independent yield function f and a viscosity parameter γ.

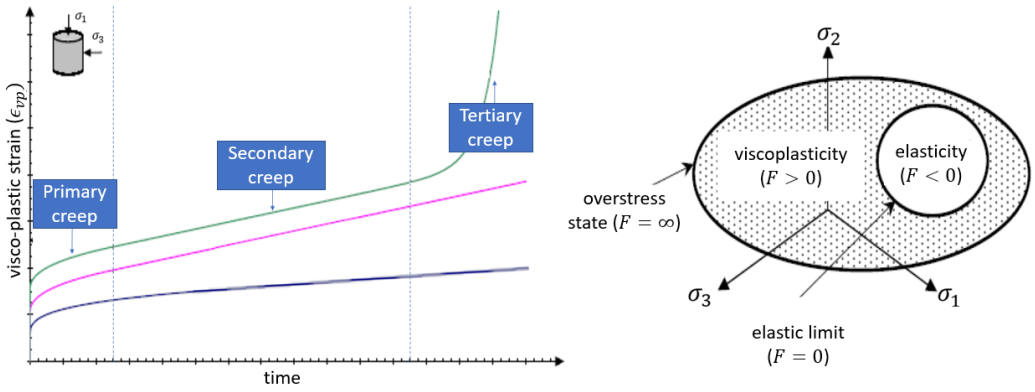

Figure 1. Representation of visco-plastic strain evolution at left. Elastic and visco-plastic domains at right.

The Norton law is described by the following equation:

$$\dot{\epsilon}_{ij}^{vp} = \frac{3}{2}(\dot{\epsilon}_{vp})\frac{s_{ij}}{q} \text{ where } \dot{\epsilon}_{vp} = \gamma < q - \sigma_s >^n \tag{2}$$

The visco-plastic strain rate is constant when the deviatoric stress does not vary. Moreover, it is important to highlight that this rate does not depend on the strength mobilization. Consequently, the visco-plastic strain rate of a ground volume close to the failure will be less than those of a ground volume far from the failure but subjected to a larger deviatoric stress because of the confining pressure.

The new creep law proposed in this paper is derived from the Norton law. An attempt to consider the strength mobilization has been performed. The visco-plastic strain rate is expressed as follows:

$$\dot{\epsilon}_{vp} = A \times \frac{1}{1+\left(\frac{a}{X}\right)^{\alpha}} \text{ and } X = \frac{d_1}{d_2} \tag{3}$$

Where d_1 and d_2 are presented on the Figure 2. A, a and α can be considered as three scale parameters and have been calibrated with the measurement coming from the underground research laboratory. The parameter X represents the strength mobilization:

$$X = \frac{d_1}{d_2} \tag{4}$$

The relationships to express d_1 and d_2 (Fig. 2) taking in account the initial deviatoric stress q_0 and the maximal deviatoric stress $q_{\max}$ are the following. The term $q_{\max}$ depends on the current stress state defined by the stress invariants: p, q and θ, where θ is the Lode angle expressed in terms of stress invariants J_2 and J_3.

$$\begin{cases} d_1(q) = < q - q_0 > \\ d_2(p,q,\theta) = \frac{|M(\theta) \times p + q - N(\theta)|}{\sqrt{M(\theta)^2 + (1)^2}}, M = \frac{1}{\left(\frac{3+\sin\phi}{6\sin\phi}\right)\cos(\theta) + \frac{\sqrt{3}}{3}\left(\frac{1-\sin\phi}{2\sin\phi}\right)\sin(\theta)}, N = M \times \frac{c \times \cos\phi}{\sin\phi} \end{cases} \tag{5}$$

$$\cos 3\theta = \frac{3\sqrt{3}}{2} \times \frac{J_3}{J_2^{3/2}} \tag{6}$$

When d_1 is equal to zero, the visco-plastic strain rate is supposed null and when d_2 is equal to zero (the stress state has reached the failure criterion), the visco-plastic strain rate is maximal. For stress states close to the initial stress state, this relationship implies that the visco-plastic strain rate is negligible. For stress states close to the failure, the visco-plastic strain rate is maximal. The influence of the scale parameter n is given on Figure 3 showing how the strength mobilization parameter X and the visco-plastic strain rate $\dot{\epsilon}_{vp}$ can vary according to the deviatoric stress at constant confining stress.

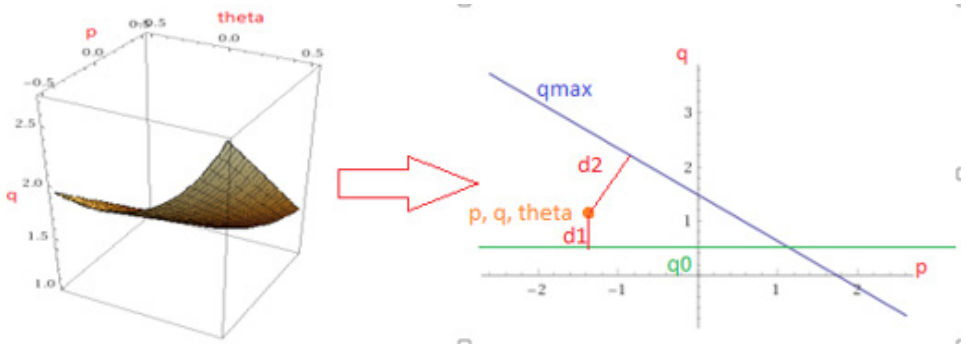

Figure 2. Representation of Mohr-Coulomb failure criterion in terms of invariants p, q, θ. Definition of the terms d_1 and d_2.

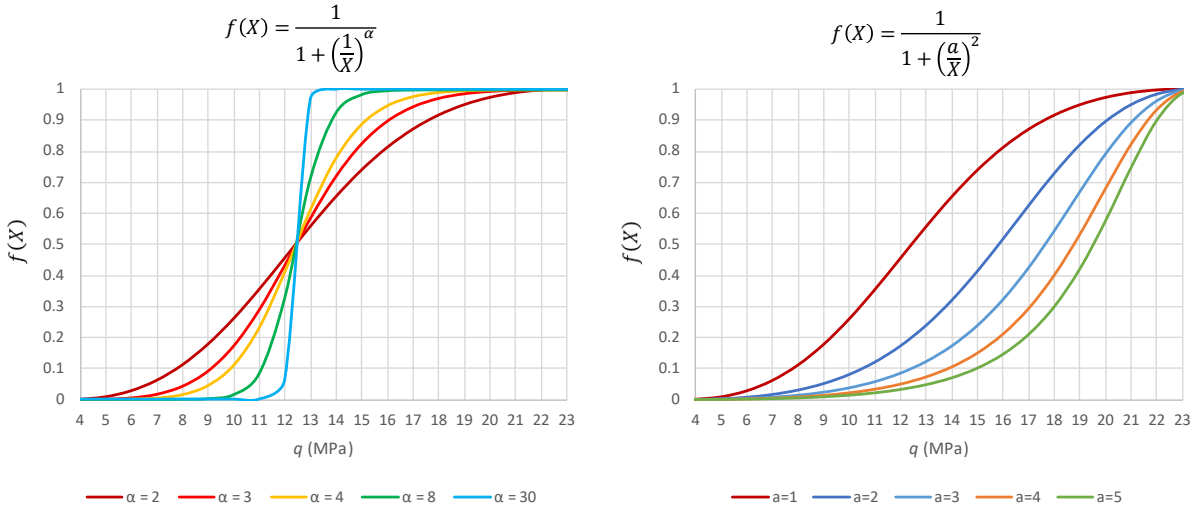

Figure 3. Influence of the parameter α ($with\ a = 1$) and a ($with\ \alpha = 2$) on the shape of the function $f(X)$, for $\theta = \pi\backslash 3,\ p = 13.8\ MPa$, $c = 6\ MPa$ and $\phi = 20°$.

3 CALIBRATION WITH MEASUREMENTS IN TERMS OF DISPLACEMENTS

The new creep law proposed in this paper is implemented in *FLAC3D* and is tested to determine the closure evolution of two galleries (GCS and GRD4, see Fig. 4 and Tables 1 & 2) of the MHM URL. Some comparisons are presented between the Norton creep law proposed by Saitta et al. 2016 and the new creep law with a Mohr-Coulomb failure criterion (Tables 3 to 5).

Soil is modeled as homogeneous and isotropic. Nevertheless, the anisotropic closure evolution observed in the URL is simulated by the adoption of an excavated damaged zone (EDZ) around the tunnel, as explicitly defined in Table 1. In this zone the cohesion, dilation angle and friction angle are different from the parameters adopted for the non-damaged soil. If we consider that radial bolts are installed in the tunnel section, the soil cohesion is greater and the angle of dilation are smaller, as showed by Table 2. Besides, an interface is considered in the model of GCS (between the support system and the soil). Finally, parameters presented in Tables 1 to 5 are adjusted so that calculated closure evolution fits the ones measured in the URL.

The progression of horizontal and vertical closure of the three galleries are presented in Figures 5 to 7. Regarding the calculated closure evolution, a comparison is made between the conventional Norton creep law, the new creep law and a semi-empirical law proposed by Sulem (1983) et Sulem et al. (1987) considering the parameters proposed by Guayacán-Carrillo (2017). These results show that the new creep law is relevant to assess displacements. For drifts excavate parallel to major stress σ_H (GCS and GRD-4), Excavation Damaged Zone evolves essentially in horizontal direction, also horizontal closure is mainly observed. Even though these tunnel sections are subjected to an almost isotropic state of stress, an anisotropic

closure evolution is constated. The behavior and characteristics of EDZ around galleries are widely discussed by Armand et al. 2014 and Saitta et al. 2016.

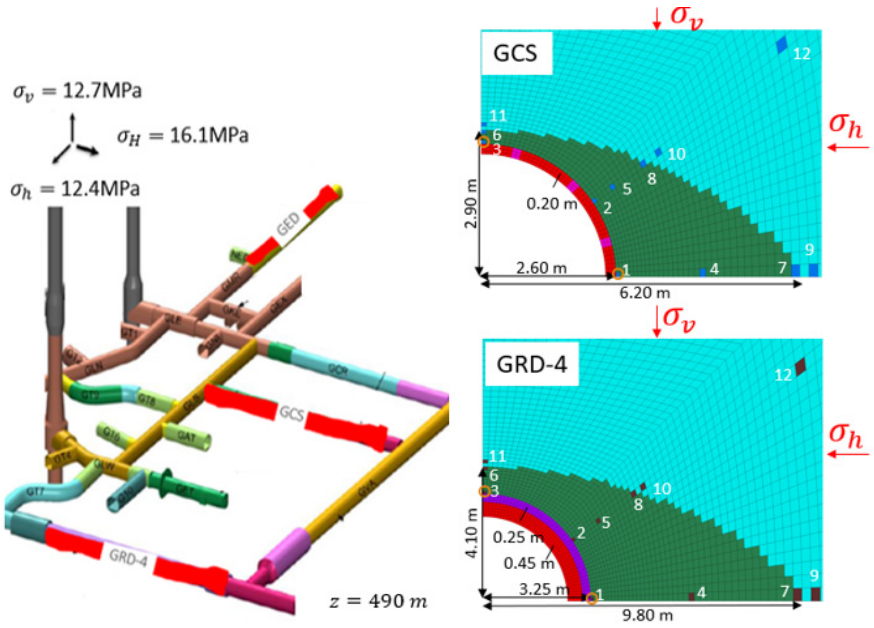

Figure 4. Representation of galleries GCS and GRD-4 in the URL. At right, sections of three galleries at *FLAC3D*. Vertical and horizontal stress are indicated as well as some points to monitor stress and strain parameters of soil.

Table 1. Equations to define the Excavated Damaged Zone (EDZ) around galleries.

Gallery	Excavation Direction	Excavation section	Limits of excavated damaged zone (EDZ)	Support system
GCS	// σ_H $(N155°E)$	Isotropic	$\left(\frac{x}{R+1.4R}\right)^2+\left(\frac{z}{R+0.10R}\right)^{1.25}=1$	Radial bolts and 20 cm of linear elastic shotcretewith 12 perfectly plastic compressible wedges of 20 x 16 cm.
GRD-4			$\left(\frac{x}{R+2.0R}\right)^2+\left(\frac{z}{R+0.25R}\right)^{1.25}=1$	No radial bolts, 25 cm of linear elastic setting mortar and 45 cm of rigid precast concrete element.
$\sigma_h = 12.4\ MPa; \sigma_H = 16.2\ MPa; \sigma_v = 12.7 MPa$				

Table 2. Adjusted parameters for two modeled galleries in *FLAC3D*.

Parameter	Non-damaged soil	Damaged soil with radial bolts	Damaged soil without radial bolts
Density ρ [kg/m³]	2450		
Young's modulus E [GPa]	4		
Poisson's ratio ν [-]	0.3		
Cohesion c [MPa]	6	0.8	0.6
Angle of dilation ψ [°]	0	2	5
Angle of friction ϕ [°]	20	25	
Traction strength σ_t [MPa]	0.9	0	

Table 3. Parameters of Norton's creep law for three modeled galleries in *FLAC3D* (Saitta et al. 2016).

$\dot{\epsilon}_{vp} = A \times < q - \sigma_s >^n$	n [-]	A $[s^{-1}Pa^{-6.8}]$	σ_s [Pa]
GCS – GRD4	6.8	2.5×10^{-59}	$q_0 = \sqrt{3\,J_{2,0}}$ (initial invariant deviatoric stress)

Table 4. Parameters of the new creep law for three modeled galleries in *FLAC3D*.

$\dot{\epsilon}_{vp}(t) = A \times \frac{1}{1 + \left(\frac{a}{(d_1)/(d_2)}\right)^{\alpha}}$	A [s^{-1}]	a [-]	α [-]
GCS – GRD4	4×10^{-11}	2	3

Table 5. Parameters of support system for three modeled galleries in *FLAC3D*.

Parameter	Density ρ [kg/m³]	Young's modulus E [GPa]	Poisson's ratio ν[-]	Other parameter
Shotcrete and setting mortar	2500	10	0	-
Compressible wedges	1100	1	-	$\epsilon_a = 40\ \%, \sigma_t = 4\ MPa$
Rigid precast concrete element	2500	39	0.3	
Interface: $k_{shear} = 200\ GPa/m$, $k_{normal} = 200\ GPa/m$, $\phi = 20°$, $c = 0$				

4 COMPARISON OF THE CONSTITUTIVE LAWS IN TERMS OF STRUCTURAL FORCES

The first calculations carried out show that some variations in terms of structural forces can be obtained according to the creep law under consideration. The bending moment variations seem quite sensitive to the choice of the creep law (Figs. 7 & 8). For example, Norton's law predicts negative bending moment along liner contrary to the new creep law that presents a change of sign. This last result is more consistent with in-situ data from galleries parallel to major stress σ_H for which intrados fiber of haunches is less compressed than extrados fiber contrary to vault and inverted vault. All these numerical results seem to show that Norton's law might induce results that are not sensible contrary to proposed law.

These results are quite important from an economic point of view since they have a direct impact on the design of the tunnel segments (thickness, class of concrete and steel ratio). Another important point to highlight is the sensitivity of the interface properties between the tunnels and the ground. These interface properties can be defined by considering many assumptions (cohesive, frictional, adherent, etc.) and may induce very strong variations regarding the bending moment values. The shear stresses transferred between the ground and the tunnel have large effects on the structural forces into the liner but are very difficult to predict.

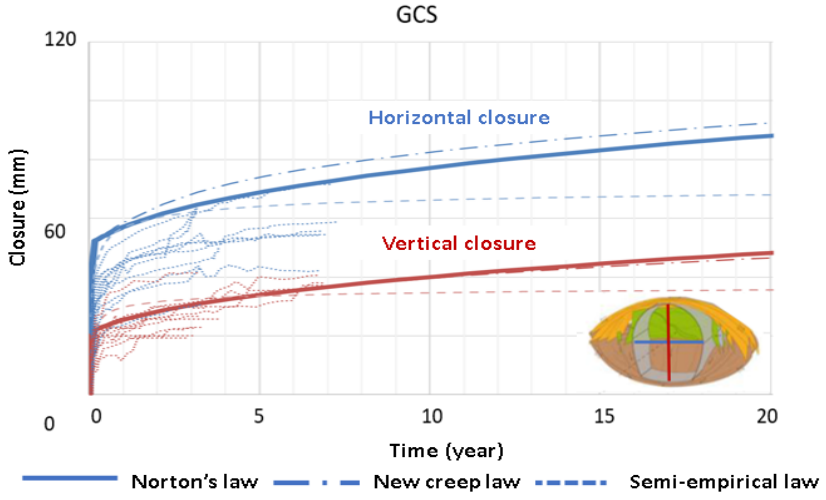

Figure 5. Comparison between calculated and measured displacement around the GCS drift. The measured values of closure in different sections of GCS drift at URL show an important dispersion, nevertheless calculated closure is fitted to extreme measured values.

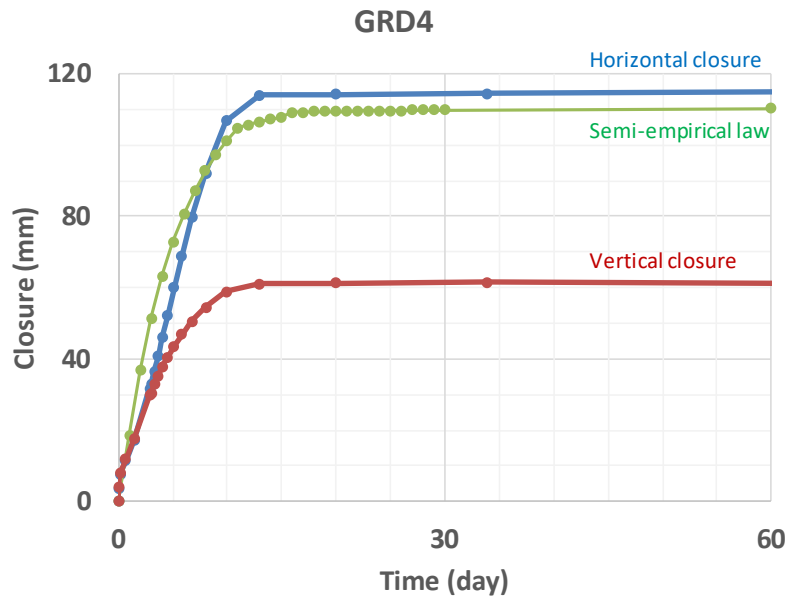

Figure 6. Comparison between calculated and measured displacement around the GRD-4 drift. Here, the measured closures are represented by the semi-empirical law proposed by proposed by Sulem (1983) et Sulem et al. (1987) considering the parameters proposed by Guayacán-Carrillo (2017). The rigid support is activated nearly about 10 days after the beginning of excavation, so that closure remains constant. Thus, the results of closure evolution calculated with Norton's law and the new creep law are the same.

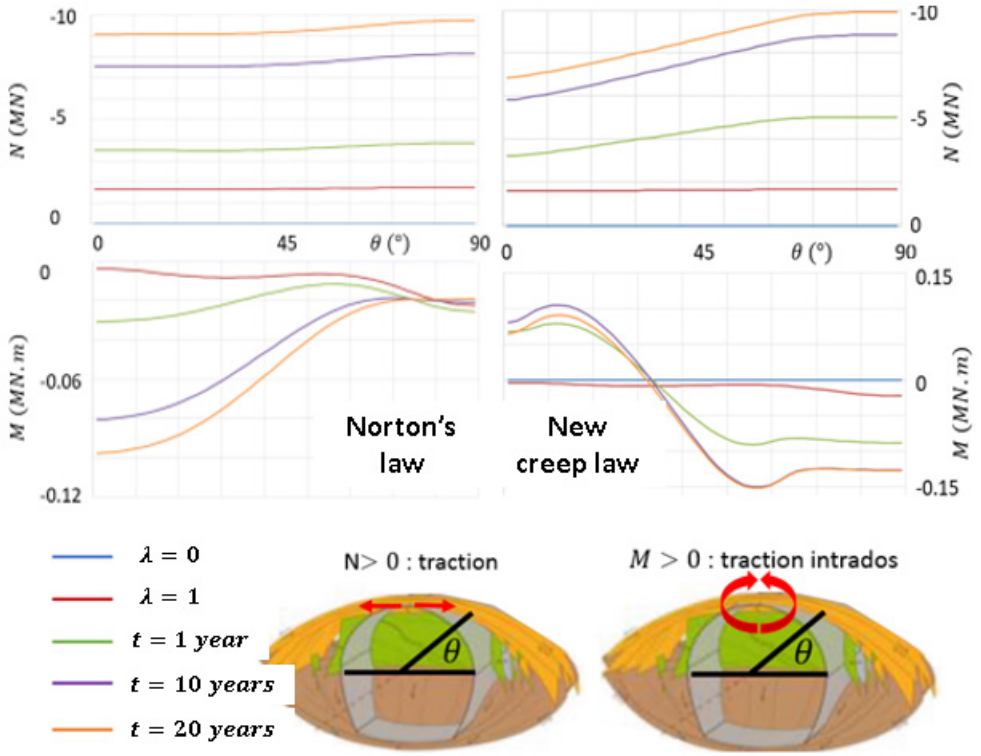

Figure 7. Normal forces and bending moments in the reinforced concrete of the GRD4 model.

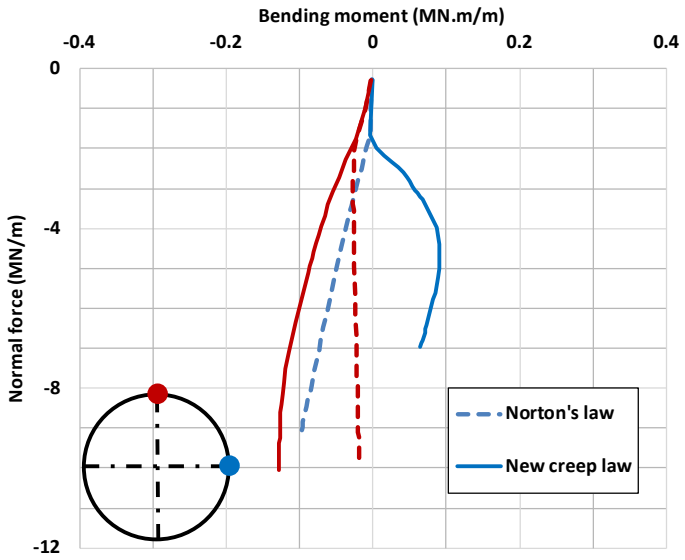

Figure 8. Comparison in the N-M interaction diagram of the two creep laws across 20 years.

5 CONCLUSIONS

This paper presents two different approaches to account for long terms effects in the design of tunnels in claystone. Differences between these two approaches are illustrated in the context of the Meuse/Haute-Marne Underground Research Laboratory (MHM URL) for two galleries parallel to major stress σ_H. Aspects related displacements and structural forces are dealt with in order to provide a broad overview of the design in terms of both ultimate limit state for the concrete elements and serviceability limit state for the displacements. This first study needs to be completed by other comparisons between measured and calculated data in order to improve interpretation of measurements and the pertinence of models.

ACKNOWLEDGEMENTS

The authors would like to thank Andra for the experimental data used in this study.

REFERENCES

Armand, G., Leveau, F., Nussbaum, C., de La Vaissiere, R., Noiret, A., Jaeggi, D., Landrein, P. & Righini, C. 2014. Geometry and Properties of the Excavation-Induced Fractures at the Meuse/Haute-Marne URL Drifts. *Rock Mech. Rock Eng*. 47, 21–41.

Boidy, E. 2002. Modélisation numérique du comportement différé des cavités souterraines. Univ. Joseph Fourier - Grenoble I 321.

Guayacán-Carrillo, L.-M. 2017. Analysis of long-term closure in drifts excavated in Callovo-Oxfordian claystone: roles of anisotropy and hydromechanical couplings. Univ. Paris Est 169.

Souley, M., Armand, G., Su, K. & Ghoreychi, M. 2011. Modeling the viscoplastic and damage behavior in deep argillaceous rocks. *Phys. Chem. Earth* 36, 1949–1959.

Sulem, J. 1983. Comportement différé des galeries profondes. ENPC, France.

Sulem, J., Panet, M. & Guenot, A. 1987. Closure Analysis in Deep Tunnels 10.

Saitta, A., Lopard, G., Petizon, T. & Armand, G. 2016. Projet Cigéo (Frans) – Modélisation du comportement des argilites de la garlerie GRD du laboratoire souterrain de Meuse/Heute-Marne.